A micro-mechanically based continuum model for strain-induced crystallization in natural rubber

CrossMark

Sunny J. Mistry, Sanjay Govindjee *

University of California, Berkeley, United States

A B S T R A C T

Recent experimental results show that strain-induced crystallization can substantially improve the crack growth resistance of natural rubber. While this might suggest superior designs of tires or other industrial applications where elastomers are used, a more thorough understanding of the underlying physics of strain-induced crystallization in natural rubber has to be developed before any design process can be started. The objective of this work is to develop a computationally-accessible micro-mechanically based continuum model, which is able to predict the macroscopic behavior of strain crystallizing natural rubber. While several researchers have developed micro-mechanical models of partially crystallized polymer chains, their results mainly give qualitative agreement with experimental data due to a lack of good micro–macro transition theories or the lack of computational power. However, recent developments in multiscale modeling in polymers give us new tools to continue this early work. To begin with, a micro-mechanical model of a constrained partially crystallized polymer chain with an extend-chain crystal is derived and connected to the macroscopic level using the non-affine micro-sphere model. Subsequently, a description of the crystallization kinetics is introduced using an evolution law based on the gradient of the macroscopic free energy function (chemical potential) and a simple threshold function. Finally a numerical implementation of the model is proposed and its predictive performance assessed using published data.

© 2013 Elsevier Ltd. All rights reserved.

1. Introduction

The study of strain-induced crystallization (SIC) in natural rubber (NR) dates back almost a century to Katz (1925). He discovered that NR underwent a transformation from an initially amorphous solid state to a semi-crystalline state when subjected to strain by means of X-ray diffraction, a method that is still state of the art. Ever since, SIC in NR has been a topic within the complex subject of rubber elasticity, not only because NR is widely used in industrial applications such as tires, seals, and medical devices, but also because its study might deepen the understanding of the Mullins' effect (Govindjee and Simo, 1991) and provide additional insight into the superior crack growth resistance of natural rubber (Le Cam and Toussaint, 2010). Despite this apparent significance, scant work has been done in the development of a micro-mechanically based continuum model of SIC in NR.

This type of modeling task typically includes a combination of three equally important parts:

1. A micro-mechanical model of a partially crystallized polymer chain.

2. A description of the crystallization kinetics in polymers, i.e. the time evolution of the degree of crystallinity within the material.

3. A micro-to-macro transition that connects micro-kinematic variables of the single chain with macroscopic continuum deformation measures.

The cornerstone was laid by Flory's statistical mechanical theory of extended chain crystallization (Flory, 1947). In this theory he uses a Gaussian distribution function to model the partially crystallized polymer chains and assumes that the crystallized part of the chain is oriented in the direction of stretch. There is no evolution of the degree of crystallinity involved, since equilibrium crystallization is assumed. All the relations in Flory's model are derived for uniaxial loading using an affine deformation assumption, which is known to result in inaccurate predictions for large deformations. Some years later, Gaylord (1976) and Gaylord and Lohse (1976) developed an improved theory of SIC with two modified assumptions. Unlike Flory, they took chain folding into account, which adds insight about crystal morphologies and orientation, and they used a non-Gaussian distribution function derived by Wang and Guth (1952) to model the polymer chains. At the same time another model was proposed by Smith (1976). He relaxed Flory's condition that the extended crystal has to be oriented in the direction of stretch by saying that the direction a chain takes through a

* Corresponding author. Tel.: +1 510 642 6060.
  E-mail address: s_g@berkeley.edu (S. Govindjee).

crystal is determined by the first few links of a chain entrapped within the crystal itself. Other than giving good qualitative agreement with experimental data, all of the above mentioned models have the following three things in common: Firstly, all of them develop a detailed micro-mechanical model of a partially crystallized polymer chain. Secondly, only equilibrium crystallization is assumed and thus the time evolution of crystallinity is not considered. Thirdly, all of them lack a satisfactory micro-to-macro transition.

Crystallization kinetics itself is a widely studied phenomenon, e.g. in the study of phase changes in metals. Roughly speaking there are three different approaches. One of the most extensively used approaches to describe the process of crystallization is the model of Avrami (1939, 1940, 1941). Based on geometric considerations of nucleation and crystal growth, the equation of Avrami is given by the exponential law $\omega \propto 1 - e^{-kV_t}$, where ω is the degree of crystallinity, k is the average density of nuclei, and V_t is the volume a crystal would occupy after a time t. Here V_t depends on the growth rate and the shape of the crystal. Some years later a similar equation was obtained by Evans (1945) and applied to temperature-induced crystallization of Nylon 6,6 by Allen (1952). Gent (1954) was the first to extend the treatment of Avrami to stretched natural rubber vulcanizates and approximate the time functions governing crystal growth. Another widely used approach is taken by Becker (1938), Turnbull and Fisher (1949) and Hoffman and Weeks (1962). They use an Arrhenius equation to describe the crystallization process, $\dot{\omega} \propto \exp(-\Delta F/(k_B T))$, where $\dot{\omega}$ is the rate of crystallization and ΔF the free energy change upon crystallization. A third approach first discussed for polymer crystallization by Roe and Krigbaum (1965) is based on a micro-mechanical model of a partially crystallized polymer chain and uses its free energy gradient (chemical potential) $\dot{\omega} \propto -\partial F/\partial \omega$ as the driving force for crystallization.

The lack of a satisfactory micro-to-macro transition has also been a challenging topic within the micro-mechanically based modeling of rubber elasticity. A good overview of constitutive models can be found in Boyce and Arruda (2000). More recently Miehe et al. (2004) have extended the micro-plane model of Bazant and Oh (1985) to the so-called non-affine micro-sphere model of rubber elasticity. This is a microscopically motivated finite deformation model for rubberlike materials. The model combines three special features: Firstly, it includes a non-affine stretch component, where micro and macro stretches are linked through a fluctuation field on a micro-sphere. The fluctuation field itself is determined by a minimization of a microstructural free energy. Secondly, polymer cross-links and entanglements are also considered using the so-called tube model of rubber elasticity, where the movement of a single chain is restricted by a tube-like constraint (Doi and Edwards, 1986). Thirdly, since closed-form solutions to the averaging integrals over a sphere are not available, a 21-point integration scheme, as derived in the original micro-plane model of Bazant and Oh (1985), is used.

The objective of this work is to leverage these ideas and develop a computationally-accessible micro-mechanically based continuum model, that is able to predict the macroscopic behavior of NR. The derivation of this model parallels the steps in Miehe and Göktepe's non-affine micro-sphere model with select changes: Firstly, on the microscopic level the free energy of a partially crystallized unconstrained single chain is considered instead of a fully amorphous chain. The model used for the chain will be a modified version of Smith (1976), which provides a way of modeling a semi-crystalline chain with extended crystals (Section 3). The microscopic model is connected to the macroscopic level using the non-affine micro-sphere model (Section 4). Secondly, on the macroscopic level an evolution law for the degree of crystallinity based on the macroscopic free energy is introduced, where the free energy gradient is used as a driving force (Roe and Krigbaum, 1965) (Section 2). Moreover, a threshold function for the evolution law inspired by phase change evolution in martensitic alloys (Govindjee and Miehe, 2001) is introduced. Thirdly, the numerical implementation using a return mapping algorithm is explained in Section 6. Finally in Section 7 the model is discussed and the predictive performance of the proposed model assessed along with a comparison to the work of Kroon (2010).

2. Macroscopic setting of model

At the macroscopic scale the model assumes a free energy function that depends on the right Cauchy–Green deformation tensor $\mathbf{C}$ and the internal variable ω, a macroscopic measure of the degree of crystallinity in the material:

$$\Psi = \Psi(\mathbf{C}; \omega). \tag{1}$$

Following the argument that the mechanical dissipation cannot be negative (see e.g. Coleman and Noll, 1963, Truesdell and Noll, 1965, Section 79, or Simo and Hughes, 1998)

$$\mathscr{D}_{mech} = \frac{1}{2} \mathbf{S} : \dot{\mathbf{C}} - \dot{\Psi} \geqslant 0, \tag{2}$$

the second Piola–Kirchhoff stress is given by

$$\mathbf{S} = 2 \frac{\partial \Psi}{\partial \mathbf{C}}, \tag{3}$$

with the additional condition

$$-\frac{\partial \Psi}{\partial \omega} \dot{\omega} \geqslant 0. \tag{4}$$

The evolution of the degree of crystallinity is chosen to be governed by the macroscopic free energy function by setting the rate of the degree of crystallinity to

$$\dot{\omega} = -A \frac{\partial \Psi}{\partial \omega}, \quad A \geqslant 0, \tag{5}$$

where the free energy gradient acts as a driving force for the crystallinity. The condition $A \geqslant 0$ immediately follows from inserting Eq. (5) into Eq. (4). The degree of crystallinity however, can only evolve once a certain chemical potential threshold is reached. In order to incorporate this into the model, a chemical potential "yield function" of the form

$$g = \left| \frac{\partial \Psi}{\partial \omega} \right| - (g_c + \gamma \omega) \leqslant 0 \tag{6}$$

is introduced, where $g_c \geqslant 0$ (threshold at zero degree of crystallinity) and γ (hardening/softening parameter) are material constants. As long as $g < 0$, the degree of crystallinity does not evolve; i.e. $Ag = 0$.

Following common practice, a decoupling of the free energy function into volumetric and isochoric parts is introduced by use of the unimodular part of the deformation gradient (Flory, 1961)

$$\bar{\mathbf{F}} := J^{-1/3} \mathbf{F}, \quad J = \det \mathbf{F} \tag{7}$$

and using the form

$$\Psi = \Psi_{\text{vol}}(J) + \bar{\Psi}(\bar{\mathbf{C}}; \omega), \quad \bar{\mathbf{C}} = \bar{\mathbf{F}}^T \bar{\mathbf{F}}, \tag{8}$$

with volumetric and isochoric contributions to the free energy function. Applying (3) to the decoupled macroscopic free energy leads to the standard result in compressible hyperelasticity (see e.g. Holzapfel, 2000, Chapter 6)

$$\mathbf{S} = J \Psi'_{\text{vol}}(J) \mathbf{C}^{-1} + J^{-2/3} \left(\mathbb{I} - \frac{1}{3} \mathbf{C}^{-1} \otimes \mathbf{C} \right) : 2 \frac{\partial \bar{\Psi}(\bar{\mathbf{C}}; \omega)}{\partial \bar{\mathbf{C}}}. \tag{9}$$

The volumetric response $\Psi_{\text{vol}}(J)$ can be any scalar valued function which is strictly convex, has unbounded value as $J \to 0$ and

$J \to \infty$, and has a unique minimum at $J = 1$. In the next two sections, the isochoric response of the material, $\bar{\Psi}(\bar{\mathbf{C}}; \omega)$, is developed by first considering a micro-mechanical model of a partially crystalline chain and then bridging scales using the non-affine micro-sphere model.

3. Micro-mechanical setting of model

In order to develop an expression for the total free energy ψ on the micro-mechanical scale, two changes have to be made to the classical statistical mechanical treatment of polymers (see e.g. Weiner, 1983, Chapter 5). Firstly, instead of a fully amorphous polymer chain, a semi-crystalline polymer chain will be considered. Secondly, in order to account for hindrances to the motion of a single chain within a polymer network, the chain is assumed to be confined to a tube (Miehe et al., 2004). To this end, an additive split of the total free energy ψ into a contribution due to the unconstrained partially crystallized single chain ψ_f, and a contribution due to the tube constraint ψ_c

$$\psi = \psi_f + \psi_c \tag{10}$$

is assumed. In the following two subsections analytical expressions for the free energy of an unconstrained partially crystallized single chain ψ_f and the free energy of the tube constraint ψ_c are developed.

3.1. Free energy of an unconstrained partially crystallized single chain

In order to find the free energy of a *fully amorphous single chain*, typically its entropy needs to be calculated first, which in turn needs a probability density for the end-to-end vector $\mathbf{r}$ of the chain. The most common way of finding an approximation to that function is by the so-called freely jointed chain model (Wang and Guth, 1952), where a real chain is modeled by a large number of small rigid segments joined together by hinges, which allow complete freedom of orientation. In other words the problem is simplified to a random walk of N steps where each step is of length b and the endpoint of each step is uniformly distributed on a sphere of radius b. The result for the distribution function for $\mathbf{r}$ turns out to be a Gaussian distribution

$$p(\mathbf{r}) = \left[\frac{3}{2\pi N b^2}\right]^{\frac{3}{2}} \exp\left\{-\frac{3r^2}{2Nb^2}\right\} \tag{11}$$

for $r \ll Nb$, where $r = |\mathbf{r}|$. It is well known that a Gaussian distribution will result in a linear force-extension relation, often referred to as a linear entropic spring. However, at high levels of stretch the force-extension relation is known to be non-linear, where a characteristic upturn due to the limited extensibility of polymer chains is observable (Mark, 1981). In order to capture this stiffening behavior at high stretches, a non-Gaussian distribution function of the form

$$p(\mathbf{r}) = \left[\frac{3}{2\pi N b^2}\right]^{\frac{3}{2}}$$
$$\times \exp\left\{-\frac{3r^2}{2Nb^2}\right\}\left\{1 - \frac{3}{4N} + \frac{3r^2}{2N^2b^2} - \frac{9r^4}{20N^3b^4}\right\} \tag{12}$$

is derived in Wang and Guth (1952). Given the probability density $p(\mathbf{r})$ of the chain, the entropy can be calculated from Boltzmann's equation as

$$s := k \ln p, \tag{13}$$

where k is the Boltzmann constant and the free energy is then simply obtained as

$$\psi := -Ts = -kT \ln p, \tag{14}$$

where $T > 0$ is the absolute temperature.

In order to set up the *free energy of an unconstrained partially crystallized single chain* ψ_f, an approach from Smith (1976) can be adapted. Crystallization is assumed to happen as depicted in Fig. 1, where the chain has a rigid extended crystal part, two amorphous subparts, and is composed of N links each of length b. The amorphous subchains $\mathbf{r}_1$ and $\mathbf{r}_2$ consist of N_1 and N_2 links, and the crystallized part of the chain contains n links, such that $|\mathbf{l}| = nb$ and $N_1 + N_2 = N - n$. Since the crystal within the chain is assumed to be rigid, the free energy only consists of two contributions: a pure thermodynamic part and an elastic part

$$\psi_f := -\Delta H_u \left(1 - \frac{T}{T_m^0}\right) N\omega + \Delta F_e, \tag{15}$$

where ΔH_u is the heat of fusion per link, T_m^0 is the crystallization temperature, ΔF_e is the elastic contribution, and the parameter ω is the degree of crystallinity defined as

$$\omega := \frac{n}{N}, \quad \omega \in [0, 1]. \tag{16}$$

Note that ΔH_u represents, in the spirit of Flory (1947), the total (internal) energy to bring a link into the crystal. This includes both the traditional energy of fusion as well as amorphous-crystalline interface energies (which are expected to be small). The heat of fusion is an admittedly crude modeling device and properly should be viewed as an effective material parameter.

In order to calculate ΔF_e, the overall probability density p_f of the conformation in Fig. 1 is calculated as the product of the two probability densities p_1 and p_2 of the amorphous subchains

$$p_f(\mathbf{r}_1, \mathbf{r}_2) := p_1(\mathbf{r}_1)p_2(\mathbf{r}_2). \tag{17}$$

Using the kinematic relation $\mathbf{r}_2 = (\mathbf{r} - \mathbf{l}) - \mathbf{r}_1$, $\mathbf{r}_2$ is eliminated from $p_f(\mathbf{r}_1, \mathbf{r}_2)$, resulting in

$$\hat{p}_f(\mathbf{r}_1, \mathbf{r}) := p_f(\mathbf{r}_1, (\mathbf{r} - \mathbf{l}) - \mathbf{r}_1). \tag{18}$$

Since $\mathbf{r}_1$ is unknown, it is eliminated by integrating $\hat{p}_f(\mathbf{r}_1, \mathbf{r})$ over all possible values of $\mathbf{r}_1$ for fixed $\mathbf{r}$ and $\mathbf{l}$. Thus, we get

$$\tilde{p}_f(\mathbf{r}) := \int_{\mathbb{R}^3} \hat{p}_f(\mathbf{r}_1, \mathbf{r}) \, d\mathbf{r}_1. \tag{19}$$

Here, $\tilde{p}_f$ is the probability density of the conformation in Fig. 1, irrespective of the values of $\mathbf{r}_1$ and $\mathbf{r}_2$ in Eq. (17). Both, the Gaussian (11) and the non-Gaussian (12) probability densities are considered in what follows. For the *Gaussian model*, where the probability densities for the amorphous subchains p_1 and p_2 are Gaussian, a straightforward calculation leads to

$$\tilde{p}_f(\mathbf{r}) = \left(\frac{3}{2Nb^2\pi(1-\omega)}\right)^{3/2} \exp\left[-\frac{3(\mathbf{r} - \mathbf{l})^2}{2Nb^2(1-\omega)}\right]. \tag{20}$$

Assuming that the crystal $\mathbf{l}$ has the same direction as $\mathbf{r}$, the probability density can be rewritten as
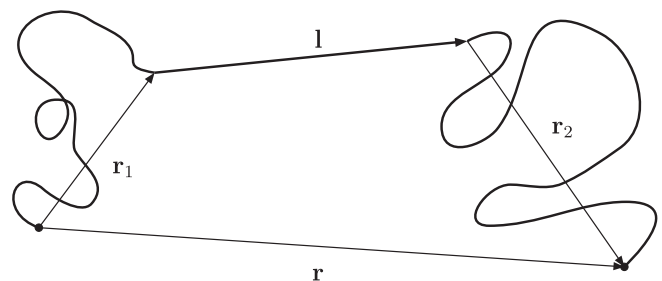
Fig. 1. Schematic of a partially crystallized chain between two crosslinks with end-to-end vectors of the two amorphous subchains $\mathbf{r}_1, \mathbf{r}_2$, the crystal vector $\mathbf{l}$, and the chain end-to-end vector $\mathbf{r}$.

$$\bar{p}_f(\lambda;\omega) = \left(\frac{3}{2Nb^2\pi(1-\omega)}\right)^{3/2} \exp\left[-\frac{3\left(\lambda-\sqrt{N}\omega\right)^2}{2(1-\omega)}\right], \quad (21)$$

where the micro-kinematic stretch λ is defined as

$$\lambda := \frac{r}{r_0}, \quad r_0 = \sqrt{N}b; \quad \lambda \in \left[0, \sqrt{N}\right]. \quad (22)$$

Thus, combining Eqs. (14) and (21), the elastic contribution reads

$$\Delta F_e = -kT\ln\left(\bar{p}_f(\lambda;\omega)\right) \quad (23)$$

and the free energy of an unconstrained partially crystallized chain (15) has the form

$$\psi_f(\lambda;\omega) := -\Delta H_u\left(1 - \frac{T}{T_m^0}\right)N\omega - \frac{3kT}{2}\left[\ln\left(\frac{3}{2Nb^2\pi(1-\omega)}\right) - \frac{\left(\lambda-\sqrt{N}\omega\right)^2}{(1-\omega)}\right]. \quad (24)$$

The derivation of the results for the *Non-Gaussian model*, where the probability density for the amorphous subchains is non-Gaussian (12), is more involved and the expression for $\bar{p}_f$ can be found in Appendix A.

Remark 1. The probability density in Eq. (21) is invariant with respect to changes in position of the extended chain crystal within the single chain. This translational invariance implies that the partially crystallized chain model in Fig. 1 is equivalent to a single chain consisting of a crystalline part and only one amorphous part.

Remark 2. It should be noted that no straining of the crystal is permitted in the model. In natural rubber, our system of interest, crystallinity is rarely greater than 20%. Thus the crystals, which are substantially stiffer than the surrounding amorphous material, experience low (relative) loads and store little strain energy as the bulk of the motion is accommodated by the softer surrounding material.

3.1.1. Free energy due to tube constraint

The tube constraint in our model is introduced following Miehe et al. (2004). The probability density due to the constraint is given by

$$p_c = p_0 \exp\left[-\alpha\left(\frac{r_0}{d_0}\right)^2 v\right], \quad (25)$$

where p_0 is a normalization constant, α is a numerical factor which depends on the tube geometry, and the dimensionless kinematic variable v is the micro-kinematic tube area contraction and is defined as

$$v := \left(\frac{d_0}{d}\right)^2, \quad v \in (0,\infty), \quad (26)$$

with d_0 being the initial diameter of the tube and d the current diameter. Using Eq. (14), the tube constraint free energy reduces to

$$\psi_c(v) = \alpha kTN\left(\frac{b}{d_0}\right)^2 v + \psi_0, \quad (27)$$

where ψ_0 is a constant.

4. Micro–macro transition

Given the analytical expressions for the total free energy on the microscale

$$\psi(\lambda, v; \omega) = \psi_f(\lambda;\omega) + \psi_c(v), \quad (28)$$

the isochoric contribution to the total macroscopic free energy (8) is calculated next. The additive split of the microscopic free energy ψ motivates the following macroscopic split energy

$$\bar{\Psi}(\bar{C};\omega) = \bar{\Psi}_f(\bar{C};\omega) + \bar{\Psi}_c(\bar{C}). \quad (29)$$

To connect the two expressions, a relationship between the micro-kinematic variables λ and v and macro-kinematic variables like $\bar{C}$ or $\bar{F}$ has to be established. It is important to note here that the internal variable ω is assumed to be a measure of the degree of crystallinity on the microscale as well as on the macroscale, and thus an identity map for its micro–macro transition is assumed. In the following two subsections the core result of the non-affine micro-sphere model (Miehe et al., 2004) is used to find the desired macroscopic free energies.

4.1. Non-affine network model for the partially crystallized chain

The main idea in the non-affine micro-sphere model is to connect the micro-kinematic variables through an averaging over a unit sphere to macro-kinematic quantities. In the case of the unconstrained partially crystallized chain the micro-stretches λ are allowed to fluctuate on the unit sphere

$$\lambda = \bar{\lambda}f(\theta, \phi), \quad (30)$$

where θ and ϕ are coordinates on the sphere, $\bar{\lambda}^2 = \mathbf{M}\cdot\bar{C}\mathbf{M}$ is the macro-stretch induced on the undeformed sphere by $\bar{C}$ in the direction of a sphere orientation vector $\mathbf{M}$ (and $\mathbf{M}\cdot\mathbf{M} = 1$), and f is a stretch-fluctuation field defined on the unit sphere. In an affine model the value of f would be unity in all unit sphere directions. However, in the non-affine model f needs to be determined; this is accomplished by requiring the following constraint to hold

$$\langle\lambda\rangle_p = \langle\bar{\lambda}\rangle_p, \quad (31)$$

where $\langle\cdot\rangle_p$ is the p-root average over the unit sphere S

$$\langle\cdot\rangle_p = \left(\frac{1}{|S|}\int_S (\cdot)^p \, dA\right)^{\frac{1}{p}} \quad (32)$$

and p is a model parameter of the micro–macro transition scheme. The macroscopic free energy for an unconstrained partially crystallized material is then determined by the minimization

$$\bar{\Psi}_f(\bar{C};\omega) = \sup_\kappa \inf_f\{\langle n_D\psi_f(\bar{\lambda}f;\omega)\rangle - \kappa(\langle\bar{\lambda}f\rangle_p - \langle\bar{\lambda}\rangle_p)\}, \quad (33)$$

where $\langle\cdot\rangle := \langle\cdot\rangle_1$ is an integration over the unit sphere, κ a Lagrange multiplier for the constraint (31), and n_D is the number of chains in the polymer network per unit volume. The necessary condition for the minimization problem is

$$n_D\frac{\partial\psi_f(\bar{\lambda}f;\omega)}{\partial\lambda} - \kappa(\langle\bar{\lambda}f\rangle_p)^{(1-p)}(\bar{\lambda}f)^{(p-1)} = 0, \quad (34)$$

which can be rewritten as

$$\kappa = n_D\frac{\partial\psi_f(\bar{\lambda}f;\omega)}{\partial\lambda}(\langle\bar{\lambda}f\rangle_p)^{(p-1)}(\bar{\lambda}f)^{(1-p)}, \quad (35)$$

where κ is constant on the sphere. Since ω is also assumed to be constant on the unit sphere, a non-trivial solution can only be derived if $\lambda = \bar{\lambda}f$ is constant. Thus, we find the simple result

$$\lambda = \langle\bar{\lambda}\rangle_p \quad (36)$$

and the macroscopic free energy contribution from the unconstrained partially crystallized chain reads

$$\bar{\Psi}_f(\bar{C};\omega) = n_D\psi_f(\langle\bar{\lambda}\rangle_p;\omega). \quad (37)$$

4.2. Non-affine network model for the tube constraint

In order to introduce a non-affine relationship between the micro-tube area contraction v as defined in Eq. (26) and a macro-area stretch on a sphere $\bar{v}$ the power law of Miehe et al. (2004) is used

$$v = (\bar{v})^q, \tag{38}$$

where $\bar{v} = \mathbf{N} \cdot \bar{\mathbf{C}}^{-1} \mathbf{N}$, and $\mathbf{N}$ is a unit normal vector to an area element on the undeformed sphere. Using the power law the macroscopic energy contribution ends up being

$$\bar{\Psi}_c(\bar{\mathbf{C}}) = \langle n_D \psi_c(\bar{v}^q) \rangle, \tag{39}$$

where q is a model parameter.

Remark 3. It should be noted that the modeling framework that has been laid out is restricted to modest degrees of crystallinity – a situation seen in NR where the maximum expected degree of crystallinity is around 20%. At higher values, say approaching 100%, one would expect the material to behave more in line with the Cauchy–Born rule (CBR); see e.g. Erickson (2008) for a recent commentary on this rule. In a general CBR motion the lattice moves affinely coupled with a non-affine basis (atom) relaxation (Weiner, 1983, Section 4.3). The micro-sphere model incorporates a relaxation but lacks a mechanism (beyond the averaging constraint) for inter-chain interactions which would allow for the "natural" appearance of CBR-like behavior. Thus the use of the micro-sphere framework for a strain crystallizing model is restricted to materials such as NR that do not exhibit large degrees of crystallization.

Remark 4. The model presented is isotropic and this warrants further discussion. When NR crystallizes it forms monoclinic crystals (Bunn, 1942a,b; Toki et al., 2003) and these are principally aligned with the loading axis (Flory, 1947; Toki et al., 2003; Guilie et al., 2013). There is clearly an *induced* anisotropy on the microscale. Since the micro-sphere framework allows one to consider independent directions it would appear that an anisotropic micro-sphere model would be possible; in fact Guilie et al. (2013) propose one such model. However, central to the micro-sphere framework is the relaxation in Eq. (33). This relaxation differentiates the micro-sphere model from the earlier efforts of, say, Treloar and Riding (1979) and Wu and van der Giessen (1993) in which affine assumptions were invoked (i.e. no relaxation) and it is what gives the micro-sphere framework its *superior* modeling capabilities. The addition of anisotropy with relaxation is non-trivial and works dealing with anisotropy and the micro-sphere model invariably assume an affine motion; see e.g. Göktepe and Miehe (2005), Menzel and Waffenschmidt (2009), or Guilie et al. (2013). In the limiting case of $\omega = 0$, the affine model is known to give a poor result; relaxation is required. The primary question is what is the appropriate variational principle to impose on the micro-sphere model during anisotropic evolution of the microstructure. With an eye towards phase transformations and plastic flow some variational principles have been developed; see e.g. Mielke (2004) and Mielke and Ortiz (2008). Unfortunately, the mathematical structure of these developments is not directly compatible with the micro-sphere framework which lacks a gradient constraint on microstructural state. Kroon (2010) in his strain crystallization model does provide one mechanism for an anisotropic relaxation but it relies on the addition of an *ad hoc* term to the micro-sphere energy. For these reasons, we choose to work with an isotropic model and view the final result as a single (isotropic) order parameter model which provides a spatially averaged measure of the true state of the material.

5. Macroscopic material response and summary

In this section the derivatives needed for the macroscopic stress–strain response are calculated and evaluated for the case of the partially crystallized single chain having a Gaussian probability density (11).

5.1. Derivatives

At this point, the contribution from the partially crystallized chain and the contribution from the non-affine tube constraint can be assembled into the overall isochoric response of the material

$$\bar{\Psi}(\bar{\mathbf{C}}; \omega) = n_D \psi_f(\langle \bar{\lambda} \rangle_p; \omega) + \langle n_D \psi_c(\bar{v}^q) \rangle. \tag{40}$$

In order to calculate the second Piola–Kirchhoff stress tensor as given in Eq. (9), the following derivative is needed,

$$\frac{\partial \bar{\Psi}(\bar{\mathbf{C}}; \omega)}{\partial \bar{\mathbf{C}}} = \frac{\partial \bar{\Psi}_f(\bar{\mathbf{C}}; \omega)}{\partial \bar{\mathbf{C}}} + \frac{\partial \bar{\Psi}_c(\bar{\mathbf{C}})}{\partial \bar{\mathbf{C}}}. \tag{41}$$

It is important to note that the derivative is taken with respect to $\bar{\mathbf{C}}$ at a constant degree of crystallinity ω. Thus, using the result in Eq. (36), the contribution from the partially crystallized chain ends up being

$$\left(\frac{\partial \bar{\Psi}_f}{\partial \bar{\mathbf{C}}} \right)_{kl} = \left(\frac{\partial \psi_f}{\partial \lambda} \frac{\partial \lambda}{\partial \bar{\lambda}} \frac{\partial \bar{\lambda}}{\partial \bar{\mathbf{C}}} \right)_{kl} = \frac{1}{2} n_D \frac{\partial \psi_f}{\partial \lambda} \lambda^{1-p} \langle \bar{\lambda}^{p-2} M_k M_l \rangle \tag{42}$$

and using (38), the non-affine tube constraint contribution results in

$$\left(\frac{\partial \bar{\Psi}_c}{\partial \bar{\mathbf{C}}} \right)_{kl} = \left(\frac{\partial \psi_c}{\partial v} \frac{\partial v}{\partial \bar{v}} \frac{\partial \bar{v}}{\partial \bar{\mathbf{C}}} \right)_{kl}$$
$$= - \left\langle n_D \frac{\partial \psi_c}{\partial v} q \bar{v}^{q-2} \frac{1}{4} (\bar{C}_{ik}^{-1} \bar{C}_{lj}^{-1} + \bar{C}_{il}^{-1} \bar{C}_{kj}^{-1}) N_i N_j \right\rangle. \tag{43}$$

The only derivatives left to evaluate are $\partial \psi_f / \partial \lambda$ from (42), $\partial \psi_c / \partial v$ from (43), and $\partial \Psi / \partial \omega$ from (5) for the evolution of the internal variable ω. For the simple case of the Gaussian probability density (11) the derivatives are listed next. The derivatives for the *Non-Gaussian model* with the probability density (12) can be calculated using the expression for $\bar{p}_f$ given in Appendix A. Using (24), the partial derivative reads

$$n_D \frac{\partial \psi_f}{\partial \lambda} = \frac{3\mu}{1-\omega} \left(\lambda - \sqrt{N}\omega \right), \quad \mu := n_D k T, \tag{44}$$

where μ, the effective shear modulus is introduced. Using (27)

$$n_D \frac{\partial \psi_c}{\partial v} = \mu N U, \quad U := \alpha \left(\frac{b}{d_0} \right)^2, \tag{45}$$

where U is the effective tube geometry parameter. The gradient in (5) is calculated using (8), and (40):

$$\frac{\partial \Psi(\bar{\mathbf{C}}; \omega)}{\partial \omega} = n_D \frac{\partial \psi_f(\langle \bar{\lambda} \rangle_p; \omega)}{\partial \omega} = -\mu_D N \left(1 - \frac{T}{T_m^0} \right)$$
$$- \frac{3\mu}{2} \left[\frac{1}{1-\omega} + \frac{2\sqrt{N}(\lambda - \omega\sqrt{N})}{1-\omega} - \frac{(\lambda - \omega\sqrt{N})^2}{(1-\omega)^2} \right]_{\lambda = \langle \bar{\lambda} \rangle_p}, \tag{46}$$

where $\mu_D := n_D \Delta H_u$ is the effective heat of fusion.

5.2. Model summary

The proposed model has a total of *eight material parameters*, summarized in Table 1, in addition to the ambient temperature T and the crystallization temperature T_m^0, which are both used in

Eq. (46). Five of the parameters are associated with the non-affine micro-sphere model and three additional parameters are introduced for the crystallization kinetics: μ_D is the heat of fusion (per unit volume); g_C is the threshold value the driving force $|\partial\Psi/\partial\omega|$ has to reach before the crystallization process can start; γ is a hardening/softening parameter, meaning that if $\gamma > 0$, the driving force threshold increases as the degree of crystallinity goes up. On the other hand if $\gamma < 0$, the driving force threshold decreases as the degree of crystallinity goes up, which in turn means that once the crystallization process has started, it becomes progressively easier for the crystallization to continue.

6. Return mapping algorithm

In this section the algorithmic setting of the proposed constitutive model for strain-induced crystallization is explained. The goal of the numerical implementation is to be able to calculate the evolution of the stress tensor and the degree of crystallinity for a given deformation cycle.

As a first step of the algorithm a trial stress tensor (9) is calculated assuming no evolution of crystallinity. In order to do so, the averaging integrals over the unit sphere in (42) and (43) have to be evaluated. This is done using a 21-point integration scheme as derived in Bazant and Oh (1986). A very thorough and easy-to-follow description of the algorithm using the 21-point integration scheme is provided in Miehe et al. (2004) and thus it is not further discussed here.

Once the trial stress tensor $\mathbf{S}_{n+1}^{trial}$ has been computed, a return mapping algorithm is proposed in order to determine the evolution of the degree of crystallinity and to correct the stress computation. The idea is to start with the trial state where the evolution of the degree of crystallinity is frozen, that is ω_{n+1}^{trial} is assumed to be the same as the previous one ω_n. Next g_{n+1}^{trial} is evaluated using ω_{n+1}^{trial} and the actual $\mathbf{C}_{n+1}$ as summarized in step 1 of Table 2. Since the trial state may or may not be a physically admissible state, the value of the threshold function g_{n+1}^{trial} is checked for consistency. If $g_{n+1}^{trial} \leqslant 0$, then no evolution of the degree of crystallinity is allowed and the trial state indeed is a physically admissible state. However if $g_{n+1}^{trial} > 0$, the trial step cannot be a solution, and there has to be an evolution of the degree of crystallinity. By numerically solving the equation $g(\mathbf{C}_{n+1}, \omega_{n+1}) = 0$ for ω_{n+1}, an admissible degree of crystallinity ω_{n+1} and an updated $\mathbf{S}(\mathbf{C}_{n+1}, \omega_{n+1})$ can be computed.

7. Numerical results and discussion

This section uses published X-ray diffraction measurements carried out by Toki et al. (2003) to test the proposed model. Moreover the proposed model is compared to the recent model of Kroon (2010) and the differences between them are discussed.

7.1. Model compared to experiments

In the experiments of Toki et al. (2003), strain-induced crystallization is measured using in situ synchrotron wide-angle X-ray diffraction on sulfur (NR-S) and peroxide (NR-P) cured natural rubber as well as sulfur vulcanized synthetic polyisoprene rubber (IR-S). The experiments are conducted at 0 °C, where a 25 mm sample is uniaxially deformed from a stretch of 1 to a stretch of 6 and back at 10 mm/min. One loading cycle thus takes approximately 25 min. The data for the NR-S, NR-P, and IR-S samples are plotted as dotted lines in Figs. 2, 3, and 4, respectively. Optimized model parameters are found in two steps. In a first step, the evolution of the degree of crystallinity from the experiments is considered as given and only the stress–strain curve is fit. An estimate of the five material parameters of the non-affine micro-sphere model (N, p, μ, q, U) is thus calculated using a least squares fit. As a next step, the remaining three parameters (μ_D, g_C, γ) are fit by hand with only minor changes of the other parameters. This is feasible because of a clear meaning of the three parameters: an increase in μ_D decreases the maximum degree of crystallinity, and slightly increases the incipient crystallization stretch; an increase in g_C increases the the incipient crystallization stretch and lowers the maximum degree of crystallinity; and an increase in γ decreases/delays incipient decrystallization stretch and slightly decreases the maximum degree of crystallinity. The optimized material parameters for the model curves are listed in Table 3.

In Fig. 2(a) Toki's experimental data for the NR-S sample is indicated by the dotted line and the prediction by the *Gaussian model* by the solid line. The prediction of the stress–strain hysteresis is in good agreement up to a stretch of 4. Above a stretch of 4, during loading, our model under predicts the stress due to the fact that our crystallization flow-rule is rate independent; this point is supported by the experimental observations of Marchal (2006). Note, that this rate dependency is independent of whether or not the background material model is elastic or viscoelastic. The prediction of the crystallization is seen to be quite good, except for the decrystallization from a stretch of 3 to 1. The prediction there appears to have some type of "inverse yielding" (necking during unloading) as mentioned in Albouy et al. (2005) and Trabelsi et al. (2003). Note a negative value of γ is used which suggests a softening as mentioned in Section 5.2. It is also important to point out that the predicted value of $N \approx 196$ is physically sound. Assuming a monomer length of $b = 4$ Å, the maximum degree of crystallinity $\omega_{max} \approx 0.15$ gives us an estimated crystallite length of $l_c \approx N\omega_{max}b \approx 118$ Å, which falls into the range of reported crystallite lengths of 80 Å to 180 Å (Chenal et al., 2007; Trabelsi et al., 2003). Lastly it is noted that no relevant differences are found between the prediction generated by the *Non-Gaussian model* in Fig. 2(b) and the *Gaussian model* in Fig. 2(a).

In Fig. 3(a) Toki's experimental data for the NR-P sample is indicated by the dotted line and the prediction by the *Gaussian model* by the solid line. The same remarks as made for the quality of the NR-S fit can be made here as well. However in Fig. 4(a) the quality of the stress–strain hysteresis fit for Toki's IR-S seems to be better than the quality of the previous two fits. Deviations are only found on the loading curve between stretches of 4 and 6. Additionally the model is able to fully capture the instant start of the decrystallization as seen in the unloading part of the

Table 1
Material parameters of the model.

#	Parameter	Name	Eq.	Effect
1	$\mu := n_D kT$	Shear modulus	(44)	Ground state stiffness
2	N	Number of chain segments	(11)	Chain locking response
3	p	Non-affine stretch parameter	(31)	3D locking characteristic
4	$U := \alpha(b/d_0)^2$	Tube geometry parameter	(45)	Additional constraint stiffness
5	q	Non-affine tube parameter	(38)	Shape of constraint stress
6	$\mu_D := n_D \Delta H_u$	Heat of fusion	(46)	Heat of fusion
7	g_C	Threshold parameter	(5)	Threshold at $\omega = 0$
8	γ	Threshold evolution parameter	(5)	Softening/hardening

Table 2
Implementation of the return mapping algorithm for strain-induced crystallization.

1	Given the deformation $\mathbf{C}_{n+1}$, compute the trial state (no evolution of crystallinity): $\omega_{n+1}^{trial} = \omega_n$ $g_{n+1}^{trial} = g(\mathbf{C}_{n+1}, \omega_n)$ $\mathbf{S}_{n+1}^{trial} = \mathbf{S}(\mathbf{C}_{n+1}, \omega_n)$
2	Check consistency of crystallization step: if $g_{n+1}^{trial} \leqslant 0$, then $(\cdot)_{n+1} := (\cdot)_{n+1}^{trial}$ & EXIT
3	else $g_{n+1}^{trial} > 0$, set $g_{n+1} = \left\| \frac{\partial \Psi(\langle \lambda \rangle_p, \omega_{n+1})}{\partial \omega} \right\| - (g_C + \gamma \omega_{n+1}) = 0$ and solve for ω_{n+1} using a Newton–Raphson scheme, where a Backward-Euler scheme is used to integrate the evolution equation: $\omega_{n+1} = \omega_n - A(t_{n+1} - t_n)(\partial \Psi(\langle \lambda \rangle_p, \omega_{n+1})/\partial \omega)$
4	Calculate the new $\mathbf{S}_{n+1}$ using the updated ω_{n+1}
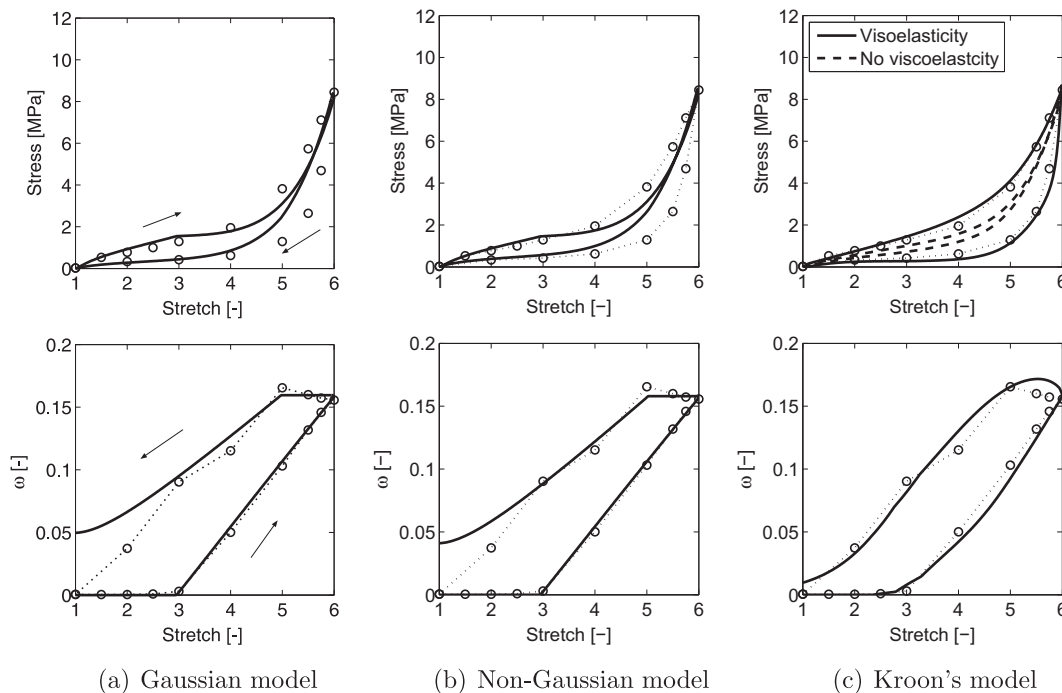
Fig. 2. Comparison of the sulfur vulcanized NR data (dotted line) to: (a) the Gaussian model; (b) the non-Gaussian model; and (c) Kroon's model with (solid line) and without (dashed line) viscoelasticity. The curve for the degree of crystallinity is only plotted once because it stays the same for both cases. Optimized parameters for (a) and (b) can be found in Table 3 under NR-S.

crystallization curve. The same also holds true for the *Non-Gaussian model* in Fig. 4(b).

7.2. Model compared to Kroon's model

As mentioned in Section 1 a similar model was recently developed by Kroon (2010). One of the core differences between the two models is in how they view the increase of the degree of crystallinity. In the proposed model the increase in crystallinity stems from the growth of the extended-chain crystallites, which is supported by Chenal et al. (2007). Kroon uses the idea of Murakami et al. (2002), where the crystallite size is thought to be constant and the growth driven by nucleation. However, it is also mentioned in Murakami et al. (2002) that the induced crystallites are well packed, which can be seen as a growing crystallite provided the definition of a crystallite is loosened a bit. In any case, researchers do not seem to fully agree on the mechanism that governs the increase in crystallinity.

Another important point is viscoelasticity. In order to be able to predict the stress–strain hysteresis, Kroon uses a phenomenological viscoelastic component. However Murakami et al. (2002) and Trab-

elsi et al., 2003 clearly note that the hysteresis is entirely due to the phenomenon of crystallization and not due to viscoelastic effects. Toki's loading rate is also observed to be rather slow. Kroon's predictions with and without the viscoelastic component are plotted in Figs. 2(c), 3(c), and 4(c). The plots show that without the viscoelastic component only a slight stress–strain hysteresis is observable. In the proposed model no viscoelastic component is used. This issue is clearly important if the model is to be utilized for fracture prediction where energy balance issues are of paramount interest.

Another difference in the models is the evolution law for the degree of crystallinity. In Kroon's model a phenomenological Arrhenius equation is implemented to govern the crystallinity. However in the proposed model it is felt that the approach using the chemical potential as a driving force is more physical and provides the better predictions for the degree of crystallinity, especially if compared in the case of IR-S in Fig. 4.

A further modeling difference is found in the way the non-affine deformation is introduced. Kroon uses a phenomenological compliance stretch on the microscopic scale to incorporate non-affine deformation. Computationally it is equivalent to the
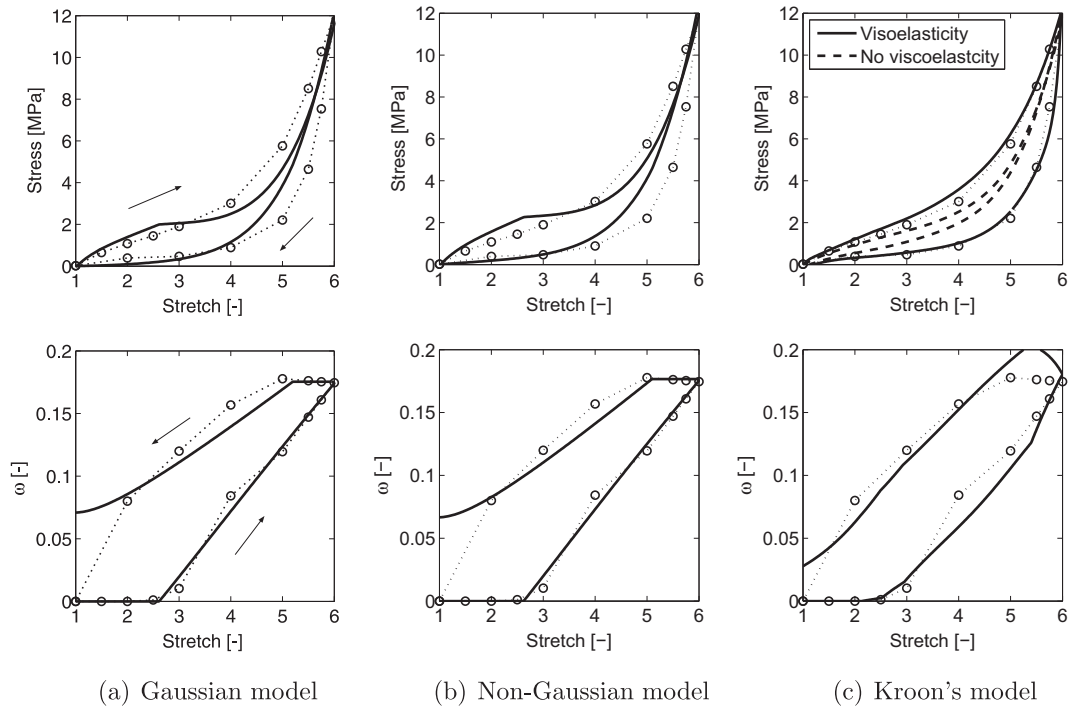
Fig. 3. Comparison of the peroxide vulcanized NR data (dotted line) to: (a) the Gaussian model; (b) the non-Gaussian model; and (c) Kroon's model with (solid line) and without (dashed line) viscoelasticity. The curve for the degree of crystallinity is only plotted once because it stays the same for both cases. Optimized parameters for (a) and (b) can be found in Table 3 under NR-P.

introduction of an *ad hoc* penalty constraint, which is used to penalize non-affine deformation. In our proposed model the non-affine deformation is derived from a principle of minimum free energy and a simple closed-form result is obtained (Miehe et al., 2004). It is noted that Kroon's methodology can lead to unstable behavior at large stretches.

As a last point, the model parameters regarding the crystallite size are mentioned. Kroon uses a parameter N as the number of participating chains in the crystallite and a parameter n_c as the number of links in the extended-chain crystal. The first value turns out to be $N = 0.1$, which is not physical and the second value is around $n_c = 11$, which is physically quite low. In the proposed
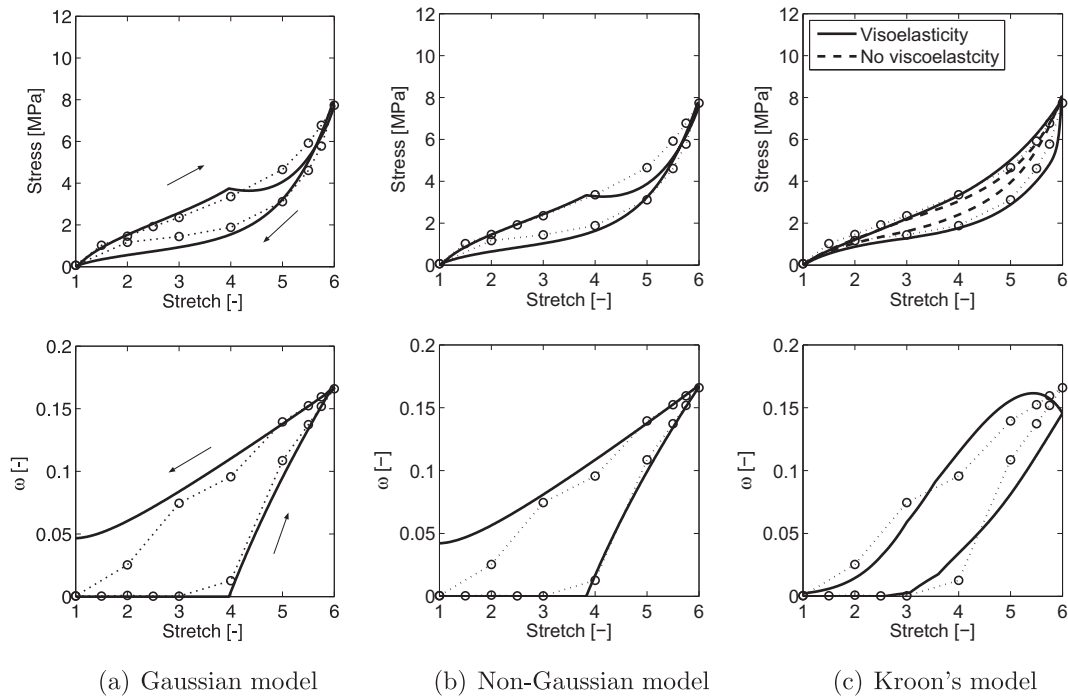
Fig. 4. Comparison of the sulfur vulcanized synthetic polyisoprene rubber data (dotted line) to: (a) the Gaussian model; (b) the non-Gaussian model; and (c) Kroon's model with (solid line) and without (dashed line) viscoelasticity. The curve for the degree of crystallinity is only plotted once because it stays the same for both cases. Optimized parameters for (a) and (b) can be found in Table 3 under IR-S.

Table 3
Optimized material parameters for the models with Gaussian and non-Gaussian probability densities. The ambient temperature is $T = 0\ ^\circ$C and the crystallization temperature is assumed to be $T_m^0 = -143.95\ ^\circ$C (isoprene).

	Gaussian model			Non-Gaussian model		
	NR-S	NR-P	IR-S	NR-S	NR-P	IR-S
N [–]	195.95	191.13	199.95	175.95	191.70	191.95
p [–]	1.4692	1.1594	1.4692	1.4692	1.4941	1.46922
μ [MPa]	0.62023	1.0191	1.02023	0.62023	1.0878	1.02023
q [–]	16.933	15.048	16.200	17.053	14.766	16.260
U [–]	3.7578e−8	1.9937e−7	3.7578e−8	3.7578e−8	2.3993e−7	3.7578e−8
μ_D [MPa]	0.110	0.125	0.210	0.115	0.130	0.205
g_C [MPa]	18	34	42	14	34	34
γ [MPa]	−65	−140	−260	−45	−120	−205

Table 4
The material parameters used for the reproduced results of Kroon's model.

		Viscoelasticity			No viscoelasticity		
		NR-P	IR-S	NR-S	NR-P	IR-S	NR-S
n	[–]	22.0	20.0	23.3	22.0	27.6	22.4
n_c	[–]	9.3	11.0	11.0	9.9	13.1	11.0
N	[–]	0.1	0.1	0.1	0.1	0.1	0.1
μ_c	[MPa]	1.05	1.20	0.60	1.00	1.35	0.6
α	[MPa]	0	0	0	0	0	0
μ_{nc}	[MPa]	180	63	170	245	270	200
μ_v	[MPa]	1	1	1	0	0	0
η	[MPa min]	0.25	0.12	0.20	–	–	–
g_c	[min^{-1}]	0.088	0.047	0.044	0.073	0.066	0.051
g_a	[min^{-1}]	0.31	0.74	0.50	0.31	0.59	0.48

model however, the predicted size of the crystallite fully agrees with experimentally reported values.

Remark 5. The predictions in Figs. 2(c), 3(c), and 4(c) are reproduced results from Kroon (2010) and might slightly differ from the original predictions, since here a 21-point integration scheme (Bazant and Oh, 1986) is used to integrate over a spherical surface instead of the 50-point integration scheme mentioned in Kroon (2010). The material parameters used for the reproduced results of Kroon's model curves are listed in Table 4.

8. Concluding remarks

It has been shown how to develop a simple computationally-accessible micro-mechanically based continuum model for strain-induced crystallization in natural rubber. As a first step, a micro-mechanical model of a constrained partially crystallized polymer chain was derived and subsequently connected to the macroscopic level using the non-affine micro-sphere model. Furthermore, a description of the crystallization kinetics was introduced using an evolution law based on the gradient of the macroscopic free energy function (chemical potential) and a simple threshold function. Key here is the addition of a softening of the critical chemical potential driving force with advancing crystallization. The predictive performance of the proposed model was shown by fitting available experimental data for various cross-linked rubber samples, and as a last step the model was compared to a recently developed constitutive model to highlight its physical features. It is seen that both the coarse scale stress–strain response is reasonably reproduced as is the internal state degree of crystallinity. Further the fitted model parameters are seen to correctly fit in the physical range seen in experiments. The good behavior observed occurs despite our rather basic isotropic crystallization model. With added experimental work and model fitting even better data matches are envisaged.

Appendix A

The probability density of the conformation in Fig. 1 using the Non-Gaussian probability density (12) is given as

$$
\begin{aligned}
\bar{p}_f(\lambda;\omega) = & -\frac{1}{3200 N^4 \pi^{3/2}(-1+\omega)^8 \sqrt{\frac{1}{N-N\omega}}} 3\sqrt{\frac{3}{2}} e^{\frac{3(\lambda-\sqrt{N}\omega)^2}{2(-1+\omega)}} (3(243\lambda^8 - 828\lambda^6(-1 \\
& +\omega) - 2346\lambda^4(-1+\omega)^2 - 900\lambda^2(-1+\omega)^3 - 485(-1+\omega)^4) \\
& -72\sqrt{N}\lambda(81\lambda^6 - 207\lambda^4(-1+\omega) - 391\lambda^2(-1+\omega)^2 \\
& -75(-1+\omega)^3)\omega - 5832N^{7/2}\lambda\omega^7 + 729N^4\omega^8 \\
& -72N^{5/2}\lambda\omega^3(-160 + \omega(480 + (-273 + 567\lambda^2 - 47\omega)\omega)) \\
& +36N^3\omega^4(-80 + \omega(240 + \omega(-171 + 567\lambda^2 + 11\omega))) \\
& -24N^{3/2}\lambda\omega(1701\lambda^4\omega^2 - 30\lambda^2(-1+\omega)(-16 + \omega(32 + 53\omega)) \\
& -(-1+\omega)^2(1120 + \omega(-2240 + 2293\omega))) + 12N(1701\lambda^6\omega^2 \\
& -225(-1+\omega)^3\omega^2 - 15\lambda^4(-1+\omega)(-16 + \omega(32 + 191\omega)) \\
& -\lambda^2(-1+\omega)^2(1120 + \omega(-2240 + 4639\omega))) - 2N^2(800 \\
& +\omega(-4800 + \omega(18720 - 25515\lambda^4\omega^2 + 270\lambda^2(-1+\omega)(-32 \\
& +\omega(64 + 37\omega)) + \omega(-42880 + \omega(55839 + \omega(-38718 \\
& +11039\omega))))))),
\end{aligned}
$$

where N_1 and N_2 are assumed to be $N(1-\omega)/2$, since the position of the extended crystal within the chain does not change the result. The probability density $\bar{p}_f$ was calculated using Mathematica.

References

Albouy, P., Marchal, J., Rault, J., 2005. Chain orientation in natural rubber, part I: the inverse yielding effect. European Physical Journal E 17, 247–259.

Allen, P., 1952. The kinetics of the crystallization of hexamethylene adipamide polymer. Transactions of the Faraday Society 48, 1178–1185.

Avrami, M., 1939. Kinetics of phase change I – General theory. The Journal of Chemical Physics 7, 1103–1112.

Avrami, M., 1940. Kinetics of phase change. II. Transformation-time relations for random distribution of nuclei. The Journal of Chemical Physics 8, 212–224.

Avrami, M., 1941. Granulation, phase change, and microstructure - kinetics of phase change. III. The Journal of Chemical Physics 9, 177–184.

Bazant, Z., Oh, B., 1985. Microplane model for progressive fracture of concrete and rock. Journal of Engineering Mechanics 111, 559–582.

Bazant, Z., Oh, B., 1986. Efficient numerical-integration on the surface of a sphere. Zeitschrift fuer Angewandte Mathematik und Mechanik 66, 37–49.

Becker, R., 1938. Die Keimbildung bei der Ausscheidung in metallischen Mischkristallen. Annalen der Physik 424, 128–140.

Boyce, M., Arruda, E., 2000. Constitutive models of rubber elasticity: A review. Rubber Chemistry and Technology 73, 504–523.

Bunn, C., 1942a. Molecular structure and rubber-like elasticity. I. The crystal structure of β gutta-percha, rubber and polychloroprene. Proceedings of the Royal Society A 180, 40–66.

Bunn, C., 1942b. Molecular structure and rubber-like elasticity. III. Molecular movements in rubber-like polymers. Proceedings of the Royal Society A 180, 82–99.

Chenal, J.-M., Chazeau, L., Guy, L., Bomal, Y., Gauthier, C., 2007. Molecular weight between physical entanglements in natural rubber: A critical parameter during strain-induced crystallization. Polymer 48, 1042–1046.

Coleman, B., Noll, W., 1963. The thermodynamics of elastic materials with heat conduction and viscosity. Archive for Rational Mechanics and Analysis 13, 167–178.

Doi, M., Edwards, S., 1986. The Theory of Polymer Dynamics. The International Series of Monographs on Physics Series. Oxford University Press Inc.

Ericksen, J., 2008. On the Cauchy–Born rule. Mathematics and Mechanics of Solids 13, 199–220.

Evans, U., 1945. The laws of expanding circles and spheres in relation to the lateral growth of surface films and the grain-size of metals. Transactions of the Faraday Society 41, 365–374.

Flory, P., 1947. Thermodynamics of crystallization in high polymers. 1. Crystallization induced by stretching. The Journal of Chemical Physics 15, 397–408.

Flory, P., 1961. Thermodynamic relations for high elastic materials. Transactions of the Faraday Society 57, 829–838.

Gaylord, R., 1976. A theory of the stress-induced crystallization of crosslinked polymeric networks. Journal of Polymer Science Part B, Polymer Physics 14, 1827–1837.

Gaylord, R., Lohse, D., 1976. Morphological changes during oriented polymer crystallization. Polymer Engineering and Science 16, 163–167.

Gent, A., 1954. Crystallization and the relaxation of stress in stretched natural rubber vulcanizates. Transactions of the Faraday Society 50, 521–533.

Göktepe, S., Miehe, C., 2005. A micro–macro approach to rubber-like materials: Part III: The micro-sphere model of anisotropic Mullins-type damage. Journal of the Mechanics and Physics of Solids 53, 2259–2283.

Govindjee, S., Miehe, C., 2001. A multi-variant martensitic phase transformation model: Formulation and numerical implementation. Computer Methods in Applied Mechanics and Engineering 191, 215–238.

Govindjee, S., Simo, J., 1991. A micro-mechanically based continuum damage model for carbon black-filled rubbers incorporating Mullins effect. Journal of the Mechanics and Physics of Solids 39, 87–112.

Guilie, J., Lê, T.-N., Le Tallec, P., 2013. Microsphere model for strain-induced crystallization in rubber. In: Alonso, G.-N. (Ed.), Proceedings of the 8th Conference on Constitutive Models in Rubbers. Taylor & Francis, San Sebastian, Espagne, pp. 467–472.

Hoffman, J., Weeks, J., 1962. Rate of spherulitic crystallization with chain folds in polychlorotrifluoroethylene. Journal of Chemical Physics 37, 1723.

Holzapfel, G., 2000. Nonlinear Solid Mechanics: A Continuum Approach for Engineering. John Wiley & Sons.

Katz, J., 1925. Was sind die Ursachen der eigentuemlichen Dehnbarkeit des Kautschuks? Kolloid-Zeitschrift 36, 300–307.

Kroon, M., 2010. A constitutive model for strain-crystallising rubber-like materials. Mechanics of Materials 42, 873–885.

Le Cam, J.-B., Toussaint, E., 2010. The mechanism of fatigue crack growth in rubbers under severe loading: The effect of stress-induced crystallization. Macromolecules 43, 4708–4714.

Marchal, J., 2006. Cristallisation des caoutchoucs chargés et non chargés sous contrainte: effet sur les chaînes amorphes. Ph.D. thesis, University of Paris XI, Orsay.

Mark, J., 1981. Rubber elasticity. Journal of Chemical Education 58, 898–903.

Menzel, A., Waffenschmidt, T., 2009. A microsphere-based remodelling formulation for anisotropic biological tissues. Philosophical Transactions of the Royal Society A 367, 3499–3523.

Miehe, C., Goktepe, S., Lulei, F., 2004. A micro–macro approach to rubber-like materials – Part I: The non-affine micro-sphere model of rubber elasticity. Journal of the Mechanics and Physics of Solids 52, 2617–2660.

Mielke, A., 2004. Deriving new evolution equations for microstructures via relaxation of variational incremental problems. Computer Methods in Applied Mechanics and Engineering 193, 5095–5127.

Mielke, A., Ortiz, M., 2008. A class of minimum principles for characterizing the trajectories and the relaxation of dissipative systems. ESAIM: Control, Optimisation and Calculus of Variations 14, 494–516.

Murakami, S., Senoo, K., Toki, S., Kohjiya, S., 2002. Structural development of natural rubber during uniaxial stretching by in situ wide angle x-ray diffraction using a synchrotron radiation. Polymer 43, 2117–2120.

Roe, R.-J., Krigbaum, W., 1965. Application of irreversible thermodynamics to the kinetics of polymer crystallization from seeded nuclei. Polymer 6, 231–236.

Simo, J., Hughes, T., 1998. Computational Inelasticity. Interdisciplinary Applied Mathematics: Mechanics and Materials. Springer Verlag.

Smith Jr., K., 1976. Crystallization of networks under stress. Polymer Engineering and Science 16, 168–175.

Toki, S., Sics, I., Ran, S., Liu, L., Hsiao, B., 2003. Molecular orientation and structural development in vulcanized polyisoprene rubbers during uniaxial deformation by in situ synchrotron x-ray diffraction. Polymer 44, 6003–6011.

Trabelsi, S., Albouy, P., Rault, J., 2003. Crystallization and melting processes in vulcanized stretched natural rubber. Macromolecules 36, 7624–7639.

Treloar, L., Riding, G., 1979. A non-Gaussian theory for rubber in biaxial strain. I. Mechanical properties. Proceedings of the Royal Society A 369, 261–280.

Truesdell, C., Noll, W., 1965. The Non-Linear Field Theories of Mechanics. Springer Verlag, New York.

Turnbull, D., Fisher, J., 1949. Rate of nucleation in condensed systems. Journal of Chemical Physics 17, 71–73.

Wang, M., Guth, E., 1952. Statistical theory of networks of non-Gaussian flexible chains. The Journal of Chemical Physics 20, 1144–1157.

Weiner, J., 1983. Statistical Mechanics of Elasticity. John Wiley & Sons Inc.

Wu, P., van der Giessen, E., 1993. On improved network models for rubber elasticity and their applications to orientation hardening in glassy polymers. Journal of the Mechanics and Physics of Solids 41, 427–456.